Rate equations description of the asymmetric double barrier electronic cooler

A Philippe, F Carosella, X Zhu, C Salhani, K Hirakawa, M Bescond, Robson Ferreira, G Bastard

Journal of Applied Physics

RESEARCH ARTICLE | SEPTEMBER 28 2023

Rate equations description of the asymmetric double barrier electronic cooler

A. Philippe ; F. Carosella ; X. Zhu ; C. Salhani; K. Hirakawa ; M. Bescond ; R. Ferreira; G. Bastard

J. Appl. Phys. 134, 124305 (2023)
https://doi.org/10.1063/5.0155720

Journal of Applied Physics ARTICLE pubs.aip.org/aip/jap

Rate equations description of the asymmetric double barrier electronic cooler

Cite as: J. Appl. Phys. **134**, 124305 (2023); doi: 10.1063/5.0155720
Submitted: 23 April 2023 · Accepted: 27 July 2023 ·
Published Online: 28 September 2023

A. Philippe,[1] F. Carosella,[1,a)] X. Zhu,[2] C. Salhani,[2,3] K. Hirakawa,[2] M. Bescond,[4] R. Ferreira,[1] and G. Bastard[1,5]

AFFILIATIONS

[1]Laboratoire de Physique de l'École normale supérieure, ENS, Université PSL, CNRS, Sorbonne Université, Université Paris Cité, Paris F-75005, France
[2]Institute of Industrial Science, University of Tokyo, 4-6-1 Komaba, Meguro-ku, Tokyo 153-8505, Japan
[3]LIMMS-CNRS, IRL 2820, 4-6-1 Komaba, Meguro-ku, Tokyo 153-8505, Japan
[4]IM2NP CNRS Marseille, 142 Av. Escadrille Normandie Niemen, Marseille F13013, France
[5]Würzburg University Lehrstuhl für Technische Physik, Physikalisches Institut, Am Hubland, Würzburg D97074, Germany

[a)]**Author to whom correspondence should be addressed:** francesca.carosella@phys.ens.fr

ABSTRACT

Recent experimental results showed that an electron gas in an asymmetrical double barrier heterostructure can be effectively cooled down under resonant tunneling condition, thus leading to the realization of an electronic cooler. The cooling process is a multi-parameters phenomenon and it is desirable to handle this problem through a reasonably simple approach, in order to understand the role of each parameter. To this end, we present a rate equation modeling of the electron cooling. We model the resonant tunnel injection of the electrons in the well and their thermionic emission assisted by Longitudinal Optical (LO) phonons absorption and emission. The influence of several parameters on the electronic temperature is discussed. This simple model compares rather well to the predictions of non-equilibrium Green function approach and to the experiments.

I. INTRODUCTION

Increasing down-scaling of semiconductor devices leads to overwhelming power dissipation and heat production in devices (see, e.g., Refs. 1–3). Considerable efforts are being made to design heterostructures where the power consumption could be reduced.[4–9] Recently, heterostructures where the electronic temperature can be decoupled from and made lower than the lattice one were realized.[10–13] They are based on evaporative cooling which is a prerequisite process to subsequently refresh the lattice bath. As a matter of fact, NEGF simulations[14] have shown that the lattice cooling is possible but it is still quite low (few mK refrigeration) in those devices. Nevertheless, this result represents a proof of concept to validate the thermionic approach. The electron temperature is, therefore, a relevant, relatively easy to measure, physical parameter to assess the "cooling character" of the device. In this respect, the asymmetrical double barrier heterostructures under an applied external bias have proven very effective[15] since at room temperature the electronic temperature in the well could be made lower than the lattice one by several tens of degrees. In a previous study,[11] we modeled the current–voltage characteristics of a such a device. The tunneling and the thermionic currents were calculated and, requesting the current continuity in the heterostructure, allowed to compute the I(V) characteristics. We note that in such heterostructures' cold electrons are injected by resonant tunneling while hot electrons are removed by thermionic emission. Thus, it is conceivable and in fact measured[15] that this kind of evaporative cooling of the electron gas[16] leads to a lowering of its internal temperature.

A Non-Equilibrium Green Function (NEGF) analysis of the current–voltage characteristics provided a quantitative description of the cooling of the electron gas.[17] With this formalism, it is, however, very much time demanding to systematically study the cooling vs the different parameters of the system (barrier thicknesses, QW width, and barrier heights) and the physical mechanisms controlling the cooling are not so explicit.

Here, we shall present an intuitive and analytical analysis of the electron density and temperature using rate equations for the population and energy of the 2D electron gas in an asymmetric QW under an applied bias. The rate equations' approach is an already existing model which is here applied to asymmetrical double barrier heterostructures for the first time to our knowledge. Electrons constantly enter (by tunneling from the emitter or back flow from the collector near zero bias) and leave the QW (by thermionic emission or by tunnel back flowing to the emitter). Our model assumes the 2D electron gas is in a stationary state at temperature T_{QW} while the phonon bath is at equilibrium at temperature T_0 (the two temperatures model, see, e.g., Refs. 18 and 19). The stationary state is realized when the carrier concentration n_{QW} remains constant and the net power density emitted or absorbed P_{QW} by the electron gas vanishes (or the electron gas internal energy E_{QW} remains constant). These two conditions read

$$\frac{dn_{QW}}{dt} = \sum_i \left(\frac{dn_{QW}}{dt}\right)_i = 0, \tag{1}$$

$$P_{QW} = \frac{1}{S}\frac{dE_{QW}}{dt} = \sum_i (P_{QW})_i = 0, \tag{2}$$

where the summation runs over the various mechanisms that change the population and/or the energy of the electron gas. The solution of the system of the two rate equations suffices to determine both the electron temperature T_{QW} and concentration n_{QW} in the quantum well.

Within this work, we shall show that the electronic cooling does take place in biased asymmetrical double barrier structures at sufficiently high lattice temperatures to allow a strong enough evaporation of thermally excited electrons. Moreover, we shall study the dependencies of T_{QW} and nQW upon various parameters (layer thicknesses, bias, etc.). Finally, we shall show how the predictions of the rate equations model compare to the more complete NEGF model and to the experiments.

II. STRUCTURE AND MEASUREMENTS

We apply our model to a double barrier GaAs/AlGaAs heterostructure whose conduction band profile is schematically represented in Fig. 1. *Oz* is the growth axis. The left-hand side (we will refer to this region as the "emitter") is made of Si doped GaAs of doping density n_D and of an undoped thin GaAs spacer, not shown in the figure and neglected in the calculation. The emitter is followed by a thin barrier of $Al_yGa_{(1-y)}As$ of thickness L_{lb}. There is then an undoped thin GaAs QW of thickness L and a thick right-hand side (rhs) barrier of $Al_xGa_{(1-x)}As$ of thickness L_{rb}. The latter is followed by a doped GaAs region (that we will refer to as the "collector") having the same doping density as the emitter. The quantum well is thin enough to support only one bound state with confinement energy η_1. V_{lb}^0 and V_{rb}^0 are the potential barrier heights at zero applied bias. In the following, we discuss the measurements and the calculations made for two samples which differ mainly for the left-hand side (lhs) barrier thickness and height. In the following, we will refer to the two samples as sample A (lhs barrier thinner and higher) and sample B (lhs barrier thicker and lower).

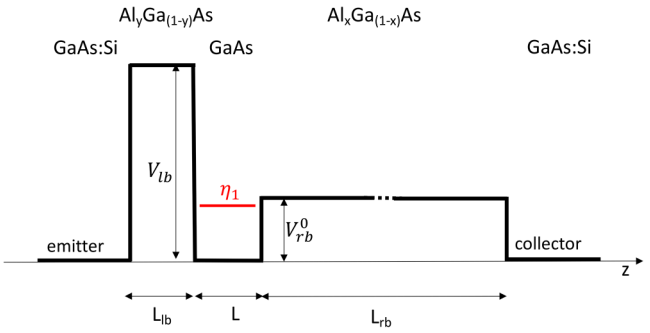

FIG. 1. Schematic representation of the conduction band profile of the double barrier heterostructure without external electric field. η_1 is the only one bound state of the QW.

The samples used in the present work were grown by molecular beam epitaxy. Sample A was prepared by growing successively on an n-type GaAs substrate, a 300 nm-thick n^+-GaAs emitter layer (Si: $1\times10^{18}\,cm^{-3}$), a 5 nm-thick undoped GaAs layer, an undoped 6 nm-thick $Al_{0.5}Ga_{0.5}As$ barrier (we call this barrier "the emitter barrier" hereafter), an undoped 6 nm-thick GaAs QW, an undoped 100 nm-thick $Al_{0.25}GaAs_{0.75}As$ barrier (we call this barrier "the collector barrier" hereafter), and a 200 nm-thick n^+-GaAs collector layer (Si: $1\times10^{18}\,cm^{-3}$). Similarly, sample B was prepared by growing successively on an n-type GaAs substrate, a 300 nm-thick n^+-GaAs emitter layer (Si: $1\times10^{17}\,cm^{-3}$), a 5 nm-thick undoped GaAs layer, an undoped 15 nm-thick $Al_{0.4}Ga_{0.6}As$ emitter barrier, an undoped 4 nm-thick GaAs QW, an undoped 100 nm-thick $Al_{0.25}GaAs_{0.75}As$ collector barrier, and a 200 nm-thick n^+-GaAs collector layer (Si: $1\times10^{18}\,cm^{-3}$). The structural parameters are summarized in Table I. The wafers were then photolithographically patterned into mesa structures with various areas, ranging from 80×80 to $800\times800\,\mu m^2$. AuGeNi/Au contacts were deposited on the front and back sides of the mesas, with the top-side including an open window to allow for optical characterization of the samples. The samples were annealed at 450 °C under an Ar atmosphere for 1 s. As a final step of the process, a 10-nm NiCr layer was deposited across the top-side window, to ensure the homogeneity of the electric field across the optical window.

We use a conduction band discontinuity between GaAs and $Ga_{1-x}Al_xAs$ equal to $V_b^0(x) = 748.3x\,meV$ and a $Ga_{1-x}Al_xAs$ effective mass of $m_b(x) = (0.07 + 0.083x)m_0$ where m_0 is the free electron mass. For the electron–phonon interaction calculations, the relative

TABLE I. Structural parameters of two double barrier heterostructures referred to as sample A and sample B.

Sample	n_D (cm^{-3})	L_{lb} (nm)	y	L (nm)	L_{rb} (nm)	x
A	10^{18}	6	0.5	6	100	0.25
B	10^{17}	15	0.4	4	100	0.25

dielectric permittivities at zero $\varepsilon_r(0)$ and infinite frequencies $\varepsilon_r(\infty)$ are taken equal to those of GaAs: $\left(\frac{1}{\varepsilon_r(\infty)} - \frac{1}{\varepsilon_r(0)}\right) = 1.42 \times 10^{-2}$. In the calculations, the zero of electrostatic potential energy and energy zero are taken at the conduction band edge of the emitter.

The electron temperature T_{QW} in the QW was extracted from photoluminescence (PL) measurements[20–22] made at different biases between the collector and the emitter. The PL measurements were carried out at 300 K. The measurements were performed by using a laser illumination at 488 nm, which corresponds to an energy of 2.54 eV. The typical laser power density we used for the measurements was 500 W cm^{-2}. The PL intensity from a QW can be expressed as $I_{QW} \propto \exp\left(-\frac{h\nu - E_0}{k_B T_{QW}}\right)$, where I_{QW} is the intensity of the PL from the QW, E_0 the energy separation of electrons and holes in the ground level, and T_{QW} the temperature of the electron system. Following this equation, T_{QW} can be extracted from a linear fit of the high-energy tail of the $\log(I_{QW})$ spectrum. This so-called linear fit method can introduce errors when the absorptivity of a material is not constant. To correct for this effect, a different method was recently developed, consisting of analyzing the ratio of a non-equilibrium spectrum over an equilibrium reference spectrum, for which the temperature is known (ratio method). In our experiment, we used the spectrum at bias V = 0 as the reference spectrum. Clear evidences of the electron cooling were obtained when the bias increases.[15]

III. MODELING

In order to determine the temperature of the electrons in the quantum well, we established and solved numerically the system of two coupled equations (1) and (2) which express the conservation of electron density [Eq. (1)] and of the internal energy of the 2D electron gas [Eq. (2)] in the QW in the presence of an applied electric field when the system is in a stationary state. The index i appearing in the summation in Eq. (1) [Eq. (2)] refers to all the physical mechanisms contributing to the change in electron population (energy) of the QW. The variation of the electron population can be due to (i1) resonant tunnel injection from the emitter, (i2) resonant tunnel back flow to the emitter, (i3) scattering-assisted thermionic emission from QW to continuum (3D above-barrier states), and (i4) scattering-assisted back flow from the collector. All the mechanisms contributing to the injection and extraction of electrons are schematically represented in Fig. 2 with the band structure in the presence of an external field F. In the figure, E_1 is the QW bound state in the presence of the external field and V_{rb} is the rhs barrier potential lowered by the field.

Assuming a parabolic dispersion for the subbands, each electron of the well contributes an energy $E_{1,\vec{k}} = E_1 + \frac{\hbar^2 k^2}{2m^*}$, with $\hbar$ the reduced Planck constant, m* the GaAs effective mass, and $\vec{k}$ the QW electron wavevector, to the internal energy of the electron gas. Thus, to account for the variation of the internal energy, on top of mechanisms (i1)–(i4), we need to include the energy exchanged by the electrons with the lattice while remaining inside the well: (i5) via longitudinal optical phonon emission and (i6) via longitudinal optical phonon absorption.

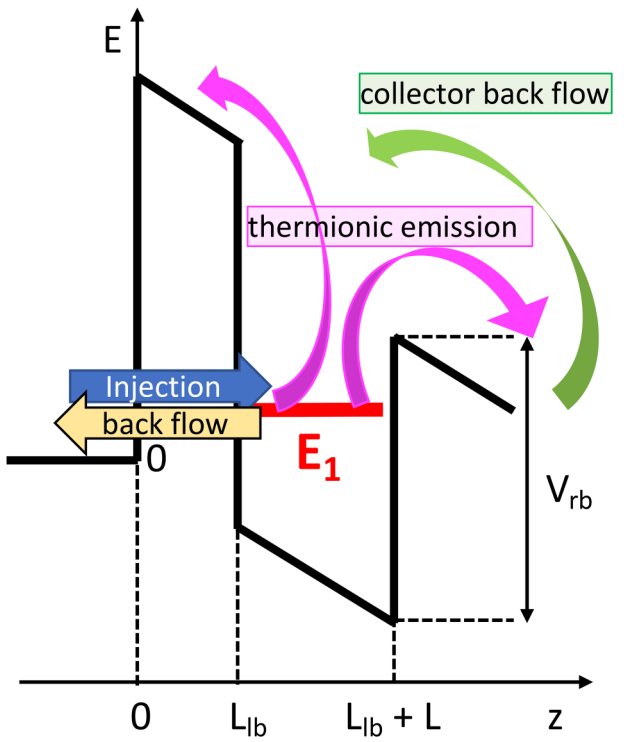

FIG. 2. Schematic representation of the double barrier heterostructure in the presence of an external electric field. All the mechanisms contributing to the injection and extraction of electrons are shown.

A. Resonant tunnel injection to QW and back flow to emitter

The resonant tunnel transfer of electrons or energy through the thin lhs barrier is modeled using Datta formalism[23,24] for the calculation of the resonant tunneling current. At the stationary state, we assume Boltzmann distribution function for the electrons in each region of the structure (emitter, QW, and collector) because the device works at room temperature. This approximation is particularly justified for the QW region, even in the presence of an applied bias, because of the very low calculated electron density ($n_{QW} \sim 10^{14}$ m^{-2}) and the elevated T_{QW} (near room temperature). The chemical potential in each region is fixed by the electron population.

In the emitter and collector, we assume that all the donors are ionized and, thus, the electron density in those regions equals the doping density n_D. Following Ref. 11, the resonant tunneling current density is, thus, given by

$$J = -\frac{em^*}{\pi\hbar^2}\frac{\Gamma(E_1)}{\hbar}\left(k_B T_{emit} e^{-\beta_{emit}(E_1-\mu_{emit})} - k_B T_{QW} e^{-\beta_{QW}(E_1-\mu_{QW})}\right) = J_{inj} + J_{bf}, \quad (3)$$

where e is the elementary charge, $\hbar$ the reduced Planck constant, k_B the Boltzmann constant, and m^* the GaAs effective mass (the same

for emitter and QW region). E_1 is the QW bound state in the presence of an electric field, and μ_{emit} and μ_{QW} are, respectively, the chemical potentials in the emitter and in the QW. T_{emit} and T_{QW} are the electron temperatures in the emitter and in the QW and $\beta_{emit} = 1/k_B T_{emit}$ and $\beta_{QW} = 1/k_B T_{QW}$. The emitter electronic temperature is taken equal to the phonon temperature T_0. $\Gamma(E_1)/\hbar$ is the tunneling rate at which an electron in the QW tunnel through the emitter barrier and in the following, we rename it as $\Gamma(E_1)/\hbar = 1/\tau_{tunnel}$. We calculate this rate by using the semiclassical model of the thermionic emission frequency of an electron, bound in the E_1 QW state, to the emitter continuum, as follows:

$$\frac{1}{\tau_{tunnel}} = \nu_{QW}(E_1)T(E_1), \tag{4}$$

where $\nu_{QW}(E_1)$ is the electron oscillation frequency in the well and $T(E_1)$ is the transmission tunneling probability through the emitter barrier. In the presence of a bias and neglecting the intra-well Stark effect on account of the small QW width (4–6 nm), the energy E_1 of the electron bound to the QW should be understood as

$$E_1 = \eta_1 - e\phi_{QW} \approx \eta_1 - eF\left(L_{bl} + \frac{L}{2}\right), \tag{5}$$

where $\eta_1 > 0$ is the zero-field electron confinement energy, ϕ_{QW} is the electrostatic potential at the center of the QW given that it is zero at the junction between the emitter and the lhs barrier, and F is the applied electric field. An electron with energy E_1 for the z motion hits the lhs wall with a frequency,

$$\nu_{QW}(E_1) = \frac{eF}{2\sqrt{2m^*}}\left(\sqrt{\eta_1 + \frac{eFL}{2}} - \sqrt{\eta_1 - \frac{eFL}{2}}\right)^{-1}. \tag{6}$$

The electron probability to tunnel through the lhs barrier $T(E_1)$ is different from zero only if the field F is such that $E_1 \geq 0$. In this condition, expression (6) is always defined since in our samples $\eta_1 \geq \frac{eFL}{2}$. Notice that relation (4) holds irrespective of the electron in plane wavevector. The first (J_{inj}) and second term (J_{bf}) of Eq. (3) refer, respectively, to the injected current density from the emitter to the well and to the current density back flow from the well to the emitter. The rate of change of the QW electron concentration due to the injection from the emitter is calculated from the first term of Eq. (3) leading to the following expression:

$$\left(\frac{dn_{QW}}{dt}\right)_{inj} = \frac{J_{inj}}{-e} = +n_D \frac{2e^{-\beta_{emit}E_1}}{\sqrt{\frac{2m^* k_B T_{emit}}{\pi\hbar^2}}} \frac{1}{\tau_{tunnel}}, \tag{7}$$

where the emitter 3D electron density is related to the chemical potential via $n_D = e^{\beta_{emit}\mu_{emit}} \frac{1}{4}\left(\frac{2m^*}{\pi\hbar^2} k_B T_{emit}\right)^{\frac{3}{2}}$. Similarly, the rate of change of the QW population density due to the back flow from the QW to the emitter can be calculated from the second term of Eq. (3), leading to the following expression:

$$\left(\frac{dn_{QW}}{dt}\right)_{emitter\ back\ flow} = \frac{J_{bf}}{-e} = -n_{QW}\frac{1}{\tau_{tunnel}}, \tag{8}$$

where the unknown n_{QW} electron density is related to the chemical potential via $n_{QW} = e^{-\beta_{QW}(E_1 - \mu_{QW})} \frac{m^*}{\pi\hbar^2} k_B T_{QW}$.

The power density P exchanged via tunneling through the left barrier is

$$P = \frac{2}{\Omega}\sum_{\vec{k}_{3D}} \mathrm{E}\left(\vec{k}_{3D}\right) \mathrm{v}_z (f_{emit} - f_{QW}) A(E_z)\Gamma(E_z), \tag{9}$$

where $\vec{k}_{3D} = \left(\vec{k}, k_z\right)$, $E\left(\vec{k}_{3D}\right) = E\left(\vec{k}\right) + E_z$ is the energy of the electron in the emitter, v_z is the electron speed along the growth axis, Ω is the emitter volume, f_{emit} and f_{QW} are the Boltzmann distribution functions, and $A(E_z)$ is the Lorenzian spectral function that we suppose sharp enough to be described by a delta function $A(E_z) = 2\pi\delta(E_z - E_1)$. As in Eq. (3), we rename $\Gamma(E_1)/\hbar = 1/\tau_{tunnel}$ and, after integration, the power density injected in the QW is given by

$$(P_{QW})_{inj} = +n_D \frac{2e^{-\beta_{emit}E_1}}{\sqrt{\frac{2m^* k_B T_{emit}}{\pi\hbar^2}}} \frac{(E_1 + k_B T_{emit})}{\tau_{tunnel}}. \tag{10}$$

Similarly, the energy loss rate associated with the electron tunnel back flow is given by

$$(P_{QW})_{emitter\ back\ flow} = -n_{QW}\frac{(E_1 + k_B T_{QW})}{\tau_{tunnel}}. \tag{11}$$

B. Scattering-assisted thermionic emission to the continuum and backflow to QW

The QW population and the associated energy also decay because of thermionic emission to the continuum assisted by the absorption or emission of LO phonons. The other scattering mechanisms (elastic scatterers and acoustical phonons) will be neglected as they were proven less efficient.[11] The lhs barrier being much taller than the rhs one, the electrons will be thermionically emitted predominantly to the continuum above the rhs low barrier. The height of the rhs potential barrier of the structure can be taylored by the external applied field as $V_{rb} = V^0_{rb}(x) - eF(L_{lb} + L)$, where $V^0_{rb}(x)$ is the zero-field rhs barrier height fixed by the Al content x. We used the Fermi golden rule to calculate the scattering time for an electron to go from an initial QW 2D state $|1, \vec{k}$ to a continuum 3D state $|\vec{k}', k'_z$ via LO phonon absorption with scattering time $\tau^{abs}_{1,\vec{k}}$ or via phonon emission scattering time $\tau^{emi}_{1,\vec{k}}$. Like in Ref. 11, the electron states are calculated using the envelope function approximation.[25] The phonon states are taken bulk-like and the electron–phonon interaction is the Fröhlich coupling. The expression of the scattering times and their determination are given in the Appendix. The QW population density decrease due to thermionic emission

can be calculated as

$$\left(\frac{dn_{QW}}{dt}\right)_{thermionic\ emi.} = -2\sum_{\vec{k}}\left(\frac{1}{\tau^{abs}_{1,\vec{k}}}+\frac{1}{\tau^{emiss}_{1,\vec{k}}}\right)f_{QW}(E_{1,\vec{k}}), \quad (12)$$

where the factor 2 takes into account the spin degeneracy and $f_{QW}(E_{1,\vec{k}})$ is the occupation function of the QW state. For a thermalized population, Eq. (12) readily becomes

$$\left(\frac{dn_{QW}}{dt}\right)_{thermionic\ emi.} = -\frac{n_{QW}}{\tau_{thermionic\ emi.}}, \quad (13)$$

with

$$\frac{1}{\tau_{thermionic\ emi.}} = \frac{\Omega C_F^2 m^*_{rb}}{8\pi^2\hbar^3}\sqrt{k_B T_{QW}}(n_{LO}e^{-\beta_{QW}(V_{rb}-E_1-\hbar\omega_{LO})}F_1^{abs}(T_{QW}) + (n_{LO}+1)e^{-\beta_{QW}(V_{rb}-E_1+\hbar\omega_{LO})}F_1^{emiss}(T_{QW})), \quad (14)$$

where

$$F_1^{abs/emiss} = \int_0^\infty dw e^{-w}\int_0^{\sqrt{w}} d\nu \int_0^{2\pi} d\theta \frac{N^{abs/emiss}(w,\nu,\theta)}{D^{abs/emiss}(w,\nu,\theta)},$$

where w and ν are dimensionless variables and the functions $N^{abs}_{emiss}(w,\nu,\theta)$ and $D^{abs}_{emiss}(w,\nu,\theta)$ are expressed in the Appendix [Eqs. (A13)–(A14)].

We define in Eq. (14) a characteristic rate for the thermionic emission where $\Omega C_F^2 = \frac{e^2\hbar\omega_{LO}}{2\varepsilon_0}\left(\frac{1}{\varepsilon_r(\infty)}-\frac{1}{\varepsilon_r(0)}\right)$, with $\varepsilon_r(0)$ and $\varepsilon_r(\infty)$ being the relative dielectric permittivities at zero and infinite frequencies, $\hbar\omega_{LO}$ the optical phonon energy, n_{LO} the Bose–Einstein occupation function at T_0, m^*_{rb} the effective mass in the rhs barrier, and V_{rb} the rhs potential barrier. Note that $1/\tau_{thermionic\ emi.}$ contains factors $\exp\left[-\frac{(V_{rb}-E_1-\hbar\omega_{LO})}{k_B T_{QW}}\right]$ that correspond to LO phonon absorption and $\exp\left[-\frac{(V_{rb}-E_1+\hbar\omega_{LO})}{k_B T_{QW}}\right]$ to LO phonon emission. These exponential activation factors make that the device will work better at elevated temperature because the extraction of the hot carriers will be the more efficient. The increase in the QW population density due to the backflow from the collector is empirically taken into account by writing

$$\left(\frac{dn_{QW}}{dt}\right)_{coll.\ back\ flow} = \frac{n_{QW}}{\tau_{thermionic\ emi.}}e^{-\beta_{coll}eFL_{rb}}, \quad (15)$$

where $\beta_{coll} = 1/k_B T_{coll}$ and we will assume the electron temperature in the collector equal to the lattice temperature ($T_{coll} = T_0$). Equation (15) ensures that the thermionic emission from the QW is exactly balanced by the thermionic emission from the collector at $F = 0$, while the backflow from the collector becomes negligible for $F > 5$–10 kV/cm.

As for the energy exchanges, there are the energy loss rates associated with the thermionic emission. They can be calculated using an approach similar to that leading to Eqs. (13)–(15) giving

$$(P_{QW})_{thermionic\ emi.} + (P_{QW})_{coll.\ back\ flow} = (n_{LO}e^{-\beta_{QW}(V_{rb}-E_1-\hbar\omega_{LO})}F_2^{abs}(T_{QW}) + (n_{LO}+1)e^{-\beta_{QW}(V_{rb}-E_1+\hbar\omega_{LO})}F_2^{emiss}(T_{QW})), \quad (16)$$

with

$$F_2^{abs}{}_{emiss} = \int_0^\infty dw(V_{rb} \mp \hbar\omega_{LO} + wk_B T_{QW})e^{-w}\int_0^{\sqrt{w}} d\nu \int_0^{2\pi} d\theta \frac{N^{abs}_{emiss}(w,\nu,\theta)}{D^{abs}_{emiss}(w,\nu,\theta)}$$

where w and ν are dimensionless variables and the functions $N^{abs}_{emiss}(w,\nu,\theta)$ and $D^{abs}_{emiss}(w,\nu,\theta)$ are the ones introduced for the thermionic emission rate [see Eqs. (A13)–(A14)].

C. Intra-well energy exchange

In addition, one needs to take into account the energy loss rates associated with the intra QW emission/absorption of LO phonons due to the difference between the electrons and phonons temperatures. This energy (density) loss rate can be calculated as

$$(P_{QW})_{intra\ QW} = \frac{2}{S}\hbar\omega_{LO}\sum_{\vec{k}}\left(\frac{1}{\tau^{abs,intra}_{1,\vec{k}}}-\frac{1}{\tau^{emiss,intra}_{1,\vec{k}}}\right)f_{QW}(E_{1,\vec{k}}) = n_{QW}\frac{\Omega C_F^2\hbar\omega_{LO}}{4\pi\hbar^2}\sqrt{\frac{m^*}{2}}\{n_{LO}-(n_{LO}+1)e^{-\beta_{QW}\hbar\omega_{LO}}\}F_3(T_{QW}), \quad (17)$$

where $\tau^{abs,intra}_{1,\vec{k}}$ $\left(\tau^{emi,intra}_{1,\vec{k}}\right)$ is the scattering time for a QW electron to go from an initial QW state $|1,\vec{k}$ to all finals QW states $|1,\vec{k}'$ via phonon absorption (emission) as expressed by the Fermi golden rule with the Fröhlich coupling. The full expression is given in Eqs. (A20)–(A23).

Notice that at zero bias, the system being at thermal equilibrium $T_{QW} = T_0$, the terms in the summation of Eq. (1) compensate each other two by two (injection and tunneling back flow on one side, and thermionic emission and thermionic back flow from collector on the other side) leading to the constant equilibrium value of n_{QW} fixed only by the doping density (via the chemical potential). Similarly, the energy loss or gain rate due to the exchanges between the well and emitter/collector is null at zero bias. Moreover, in Eq. (17), there is $\{n_{LO}-(1+n_{LO})\exp(-\beta_{QW}\hbar\omega_{LO})\} = n_{LO}\{1-\exp[(\hbar\omega_{LO})(\beta_0-\beta_{QW})]\}$, meaning that, if the electron and the phonon temperature coincide, then on average at thermal equilibrium, there is no energy gain or loss for electrons from the phonon bath as $(P_{QW})_{intra\ QW} = 0$. Our rate equation model reproduces correctly the asymptotic thermal equilibrium condition ($T_{QW} = T_0$).

IV. RESULTS

We have found that the population rates of change associated with the tunnel back flow to the emitter and the LO-assisted

thermionic emission are proportional to n_{QW}. From Eq. (1), this means that n_{QW} becomes proportional to the dopant concentration in the emitter,

$$n_{QW} = n_D \frac{\gamma}{1 + \frac{\tau_{tunnel}}{\tau_{thermionic\ emi.}}(1 - e^{-\beta_{coll} eFL_{rb}})}, \tag{18}$$

where $\gamma = 2e^{-\beta_{emit} E_1} / \sqrt{\frac{2m^* k_B T_{emit}}{\pi\hbar^2}}$. The energy loss rates are all proportional to n_{QW} but this is not the case for $(P_{QW})_{inj}$, which is proportional directly to n_D. It follows that the conservation requirement of the energy of the 2D gas is expressed by an implicit equation that no longer contains n_D. Thus, the solution T_{QW} (T_0) of Eq. (2) will also be n_D independent. This means that decreasing (increasing) the doping of the emitter would lead to inject less (more) electrons in the QW but would not change their temperature T_{QW} as long as the Boltzmann approximation is valid. This behavior may not be observed if the electron statistics in the QW or the emitter become degenerate.

As seen from Eq. (18), a good indicator of the electron cooling capability of a given asymmetric double barrier structure is given by the ratio $\frac{\tau_{tunnel}}{\tau_{thermionic\ emi.}}$. If this ratio is bigger than one, the escape of the QW electrons mainly proceeds by thermionic emission in the rhs continuum. This means that energetic carriers are more efficiently removed from the well than cold ones. Thus, the QW electron gas cools down. Note, however, that an efficient electron cooling will be accompanied by a low n_{QW}. We illustrate this trend in Fig. 3 where $\frac{\tau_{tunnel}}{\tau_{thermionic\ emi.}}$, T_{QW} and n_{QW} are calculated vs the external electric field for sample A, at various lattice temperatures T_0. Figure 3(a) shows that in this structure the thermionic emission is always a more efficient process than tunneling and that the ratio becomes larger when the external electric field increases. In fact, the electric field lowers the rhs barrier rendering the thermionic emission a faster process, thus warm electrons leave the QW faster and faster compared to cold ones. This leads to the linear and slow decrease in T_{QW} with increasing F, shown in Fig. 3(b), for three values of the lattice temperature. Thus, cooling is only possible if the electron density is low, as it can be seen from Fig. 3(c) where $n_{QW} = 0.5\text{–}2 \times 10^{14}\,\mathrm{m}^{-2}$. The steep decrease in the electron density at low field reflects the thermoactivated behavior of the electron back flow from the collector. This collector back flow becomes negligible when $F > 10\,\mathrm{kV/cm}$. In Fig. 3(b), we see the strikingly improved electron cooling upon increasing the lattice temperature T_0, which is a clear signature of the thermionic emission to the (predominantly rhs) continuum. Figure 4(a) shows the F dependence of the electron temperature T_{QW} for three QW thicknesses (all the other parameters being those of sample A and $T_0 = 300\,\mathrm{K}$). One finds the same small decrease in T_{QW} with increasing F as shown in Fig. 3(b). Increasing L decreases the zero-field confinement energy. This has two consequences. First, increasing L renders the thermionic emission to the rhs continuum less effective, which leads to a decreased cooling efficiency and, thus, to an increase in T_{QW}. Second, the critical field where E_1 passes below the emitter conduction band edge decreases with increasing L. At this field, injection stops and the thermionic emission empty the well [see Fig. 4(b)]. This explains the lack of solution $T_{QW} < T_0$ for

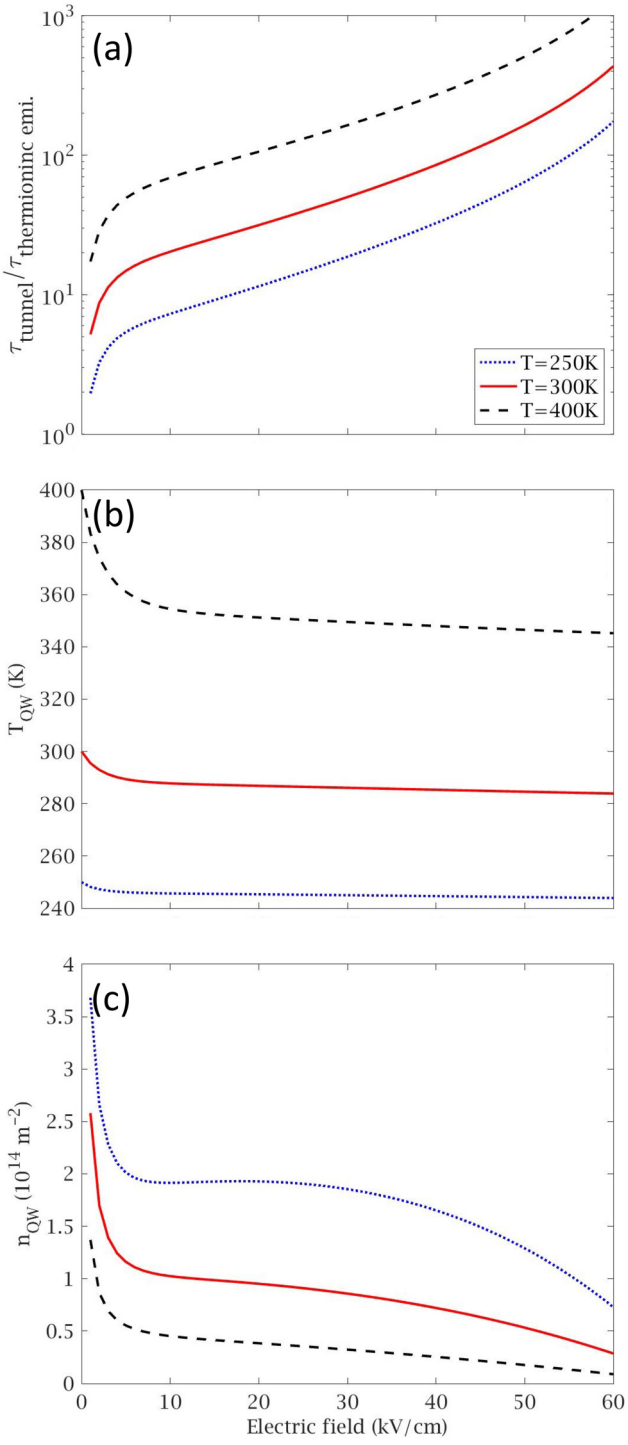

FIG. 3. (a) Ratio of characteristics times for tunneling and thermionic emission, (b) QW electronic temperature, and (c) QW electron density vs applied electric field. Calculations are done for sample A at three different lattice temperatures: $T_0 = 250\,\mathrm{K}$ (blue dots), 300 K (red line), and 400 K (black broken line).

thick wells and large F. Figure 5 shows the T_{QW} and n_{QW} dependence on the Al percentage of the rhs barrier for structures that otherwise have the same design parameters as sample A at $T_0 = 300$ K and $F = 10$ kV/cm. Increasing the Al content increases the barrier height, which limits the electron thermionic emission (n_{QW} increases) and limits the cooling (T_{QW} rises).

Finally, we show in Fig. 6 at $T_0 = 300$ K the bias dependence of the measured T_{QW} and the calculated T_{QW} either by NEGF[15] or by rate equations for sample A [Fig. 6(a)] and sample B [Fig. 6(b)]. The electric field to be introduced in the calculation is deduced from the applied bias V via the ideal capacitor model $F = V/L_{tot}$, where $L_{tot} = L_{lb} + L + L_{rb}$ is the total length of the undoped layers between the contacts. For sample A, PL measurements show that a remarkable cooling of 27 K of the electron temperature can be achieved by applying a bias of 0.4 V. Experimentally, we observe a steep decrease in the electron temperature between 0 and 2 V and then a saturation above 2 V. The rate equation model predicts the electron cooling, even if lower ($\Delta T_{QW} = 16$ K when a bias of 0.6 V is applied) than the one found experimentally, and reproduces qualitatively the cooling effect of the double barrier structure in the presence of an applied bias. Figure 6 shows also that NEGF modeling[15,17] gives an almost perfect agreement with experiments. In Fig. 6(b), we compare the results of the rate equation calculations, with the measurements and the NEGF calculations shown in Ref. 17 for sample B. Here, the predictions of the rate equations stop at the bias where E_1 passes below the emitter conduction band edge (about 0.6 V for sample B) while experimental data keep being measured far beyond that voltage. This shows that beyond 0.6 V, electrons are still supplied to the QW from the emitter. The sample B structure should indeed be very inefficient on account of the 15 nm-thick lhs barrier and it is likely that the QW feeding takes place by thermal activation above the lhs barrier rather than by direct tunneling. As shown above, the rate equation model does predict electron cooling, albeit not reaching a quantitative description of the phenomenon. The reason for such a discrepancy between the rate equation model and experiments may arise from a neglect of thermionic emission above the emitter barrier. Another aspect that deserves further investigation is the neglect of any LO phonon assisted feeding of the QW from the emitter (and its reverse process, the back flow from the QW to the emitter). Finally, the low bias behavior could also be improved by a more quantitative account of the back flow from the collector. Note, however, that significant cooling takes place only at biases such that the backflow from the collector is negligible.

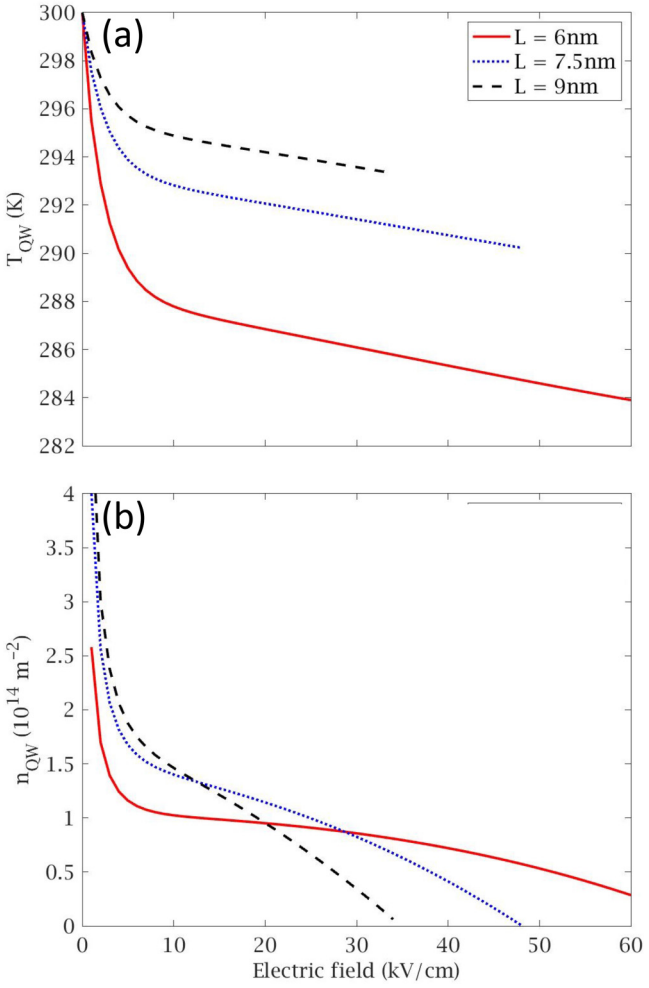

FIG. 4. (a) QW electronic temperature and (b) QW electron density vs applied electric field for various values of the QW thickness. Calculations are done at a lattice temperature $T_0 = 300$ K. The red curve corresponds to sample A (quantum well thickness L = 6 nm). For the other two curves, all the structural parameters are the one of sample A, but the QW thickness, L = 7.5 nm for the blue dotted curve and L = 9 nm for the black broken line.

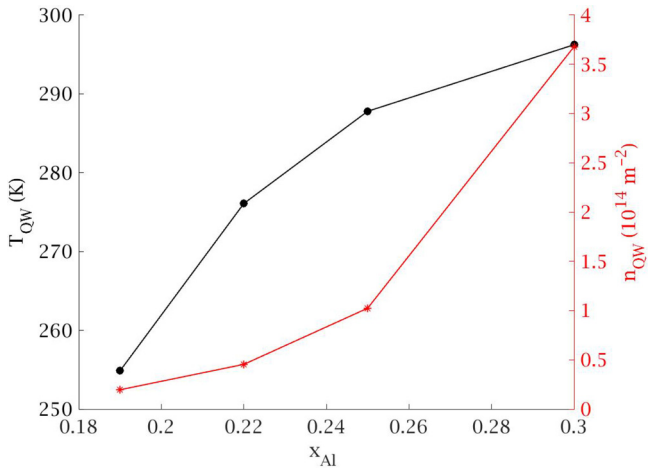

FIG. 5. QW electronic temperature and population as a function of the x_{Al} concentration. All the other parameters are those of sample A, $T_0 = 300$ K and F = 10 kV/cm.

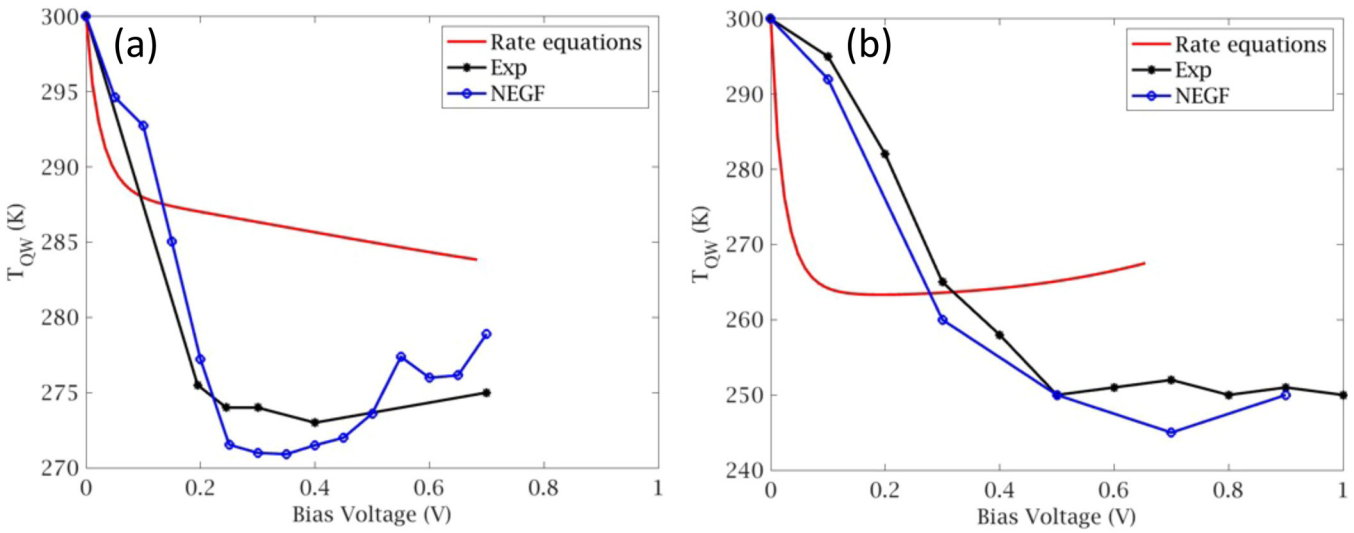

FIG. 6. QW electronic temperature vs the applied bias in sample A (a) and sample B (b). Rate equations (red) and NEGF (blue open circles) calculations are compared to experimental results (black filled circles). $T_0 = 300$ K.

V. CONCLUSION

We have reported a rate equation analysis of the electron population and temperature in an asymmetric double barrier cooling structure. We have found that an efficient electron cooling compared to the lattice temperature is always accompanied by a small ($<10^{14}$ m^{-2}) equilibrium electron concentration in the QW. Our findings are in good qualitative agreement with experiment. Despite being less precise than the NEGF technique, the rate equation approaches are much less demanding to implement than the NEGF and provide an easier grasp to the complex physical processes that control the electron cooling in semiconductor heterostructures.

ACKNOWLEDGMENTS

This work was supported by the GELATO project from ANR (No. ANR-21-CE50-0017).

AUTHOR DECLARATIONS

Conflict of Interest

The authors have no conflicts to disclose.

Author Contributions

A. Philippe: Data curation (equal); Formal analysis (equal); Investigation (equal); Software (equal); Writing – review & editing (equal). **F. Carosella:** Conceptualization (equal); Data curation (equal); Formal analysis (equal); Methodology (equal); Supervision (equal); Validation (equal); Writing – original draft (equal). **X. Zhu:** Investigation (equal). **C. Salhani:** Investigation (equal). **K. Hirakawa:** Conceptualization (equal); Resources (equal); Writing – review & editing (equal). **M. Bescond:** Conceptualization (equal); Funding acquisition (equal); Project administration (equal); Writing – review & editing (equal). **R. Ferreira:** Conceptualization (equal); Writing – review & editing (equal). **G. Bastard:** Conceptualization (equal); Formal analysis (equal); Methodology (equal); Supervision (equal); Validation (equal); Writing – original draft (equal).

APPENDIX: LO PHONON SCATTERING-ASSISTED PROCESSES

1. Thermionic emission scattering time

The electron–phonon interaction is cast in the general form

$$H_{el-ph} = \sum_{\vec{Q}_{3D}} \left[V_\alpha(\vec{Q}_{3D}) a^\dagger_{\alpha,\vec{Q}_{3D}} \exp(-i\vec{Q}_{3D}\cdot\vec{r}) + V^*_\alpha(\vec{Q}_{3D}) a_{\alpha,\vec{Q}_{3D}} \exp(i\vec{Q}_{3D}\cdot\vec{r}) \right], \quad \text{(A1)}$$

where a given phonon mode α is taken into account. $V_\alpha(\vec{Q}_{3D})$ is the coupling strength. $a^\dagger_{\alpha,\vec{Q}_{3D}}$ and $a_{\alpha,\vec{Q}_{3D}}$ are the creation and annihilation operators of a phonon in mode α and with a wavevector $\vec{Q}_{3D} = (\vec{Q}, Q_z)$. For the phonons, we take a bulk-like approach for simplicity. Here, we consider the Fröhlich coupling between the electrons and the phonons in the LO mode (supposed dispersionless) in polar materials, which is expressed by the potential,

$$V_{Fröhlich}(\vec{Q}, Q_z) = -i\frac{C_F}{\sqrt{Q^2 + Q_z^2}}, \quad \text{(A2)}$$

where C_F is the Fröhlich constant,

$$\Omega C_F^2 = \frac{e^2 \hbar \omega_{LO}}{2\varepsilon_0}\left(\frac{1}{\varepsilon_r(\infty)} - \frac{1}{\varepsilon_r(0)}\right), \tag{A3}$$

where $\Omega = SL$ is the volume of the crystal, S the surface of the sample orthogonal to the growth direction, with $\varepsilon_r(0)$ and $\varepsilon_r(\infty)$ being the relative dielectric permittivities at zero and infinite frequencies, and $\hbar\omega_{LO}$ the optical phonon energy. We assume that phonons are at thermal equilibrium described by the Bose–Einstein distribution function $n_{LO} = 1/(\exp(\beta_0 \hbar\omega_{LO}) - 1)$.

A QW electron may be scattered from an initial state $|1, \vec{k}\rangle$ to the above-barrier 3D continuum states $|\overrightarrow{k'}, k'_z\rangle$, $k_z > 0$, via the absorption or the emission of a LO phonon. We assume a structureless continuum, i.e., $\psi_{k'_z}(z) = \frac{1}{\sqrt{L_{rb}}}\exp(ik'_z z)$, $k'_z > 0$ and an asymmetric QW with $\chi_1(z)$ denoting the wavefunction associated to the bound state E_1. The scattering time due to phonon absorption or emission can be calculated using Fermi Golden rule as follows:

$$\frac{1}{\tau^{abs}_{1,\vec{k}}} = \frac{2\pi}{\hbar} n_{LO} \sum_{\overrightarrow{k'},k'_z,\overrightarrow{Q},Q_z} \frac{C_F^2}{Q^2 + Q_z^2} \left|\langle 1, \vec{k}\left| e^{i\vec{Q}\cdot\vec{\rho}} e^{iQ_z z} \right|\overrightarrow{k'}, k'_z\rangle\right|^2 \delta\left(E^{coll}_{\overrightarrow{k'},k'_z} - E_{1,\vec{k}} - \hbar\omega_{LO}\right) \tag{A4}$$

$$\frac{1}{\tau^{emiss}_{1,\vec{k}}} = \frac{2\pi}{\hbar}(n_{LO}+1) \sum_{\overrightarrow{k'},k'_z,\overrightarrow{Q},Q_z} \frac{C_F^2}{Q^2 + Q_z^2} \left|\langle 1, \vec{k}\left| e^{-i\vec{Q}\cdot\vec{\rho}} e^{-iQ_z z} \right|\overrightarrow{k'}, k'_z\rangle\right|^2 \delta\left(E^{coll}_{\overrightarrow{k'},k'_z} - E_{1,\vec{k}} + \hbar\omega_{LO}\right), \tag{A5}$$

where $E_{1,\vec{k}} = E_1 + \frac{\hbar^2 k^2}{2m^*}$ is the energy of a QW state and $E^{coll}_{\overrightarrow{k},k_z} = V_{rb} + \frac{\hbar^2 k^2}{2m^*_{rb}} + \frac{\hbar^2 k_z^2}{2m^*_{rb}}$ the energy of a continuum state above the collector (rhs) barrier. In these expressions, the summations over the phonon states lead to

$$\sum_{\overrightarrow{Q},Q_z} \frac{C_F^2 \left|\langle 1, \vec{k}\left| e^{i\vec{Q}\cdot\vec{\rho}} e^{iQ_z z} \right|\overrightarrow{k'}, k'_z\rangle\right|^2}{Q^2 + Q_z^2} = \frac{C_F^2}{Q}\frac{L}{2}\int_{-\infty}^{\infty} dz dz' \chi_1^*(z)\psi_{k'_z}(z)\chi_1(z')\psi^*_{k'_z}(z') e^{-Q|z-z'|}, \tag{A6}$$

with $Q = \sqrt{k^2 + k'^2 - 2kk'\cos(\theta)}$ and $\widehat{\vec{k}, \vec{k'}} = \theta$, which, inserted in Eqs. (A4) or (A5) and after integration on k_z', gives for phonon absorption,

$$\frac{1}{\tau^{abs}_{1,\vec{k}}} = n_{LO}\frac{\Omega C_F^2 \sqrt{2m^*_{rb}}}{16\pi^2\hbar^2}\int_0^{\infty}\frac{dk'^2}{2\sqrt{\Delta E^{abs}(k,k')}}\int_0^{2\pi} d\theta \frac{I_{abs}(Q)}{Q}\,\Theta(\Delta E^{abs}), \tag{A7}$$

with $\Delta E^{abs}(k,k') = \frac{\hbar^2 k^2}{2m^*} - \frac{\hbar^2 k''^2}{2m^*_{rb}} - V_{rb} + E_1 + \hbar\omega_{LO}$, and for phonon emission,

$$\frac{1}{\tau^{emiss}_{1,\vec{k}}} = (n_{LO}+1)\frac{\Omega C_F^2 \sqrt{2m^*_{rb}}}{16\pi^2\hbar^2}\int_0^{\infty}\frac{dk'^2}{2\sqrt{E^{emiss}(k,k')}}\int_0^{2\pi} d\theta \frac{I_{emiss}(Q)}{Q}\,\Theta(\Delta E^{emiss}), \tag{A8}$$

with $\Delta E^{emiss}(k,k') = \frac{\hbar^2 k^2}{2m^*} - \frac{\hbar^2 k'^2}{2m^*_{rb}} - V_{rb} + E_1 - \hbar\omega_{LO}$. In (A7) and (A8), there is the integral,

$$I_{abs/emiss}(Q) = \int_{-\infty}^{\infty} dz dz' \chi_1^*(z)\chi_1(z')e^{-Q|z-z'|} \times \cos\left(\sqrt{\frac{2m^*_{rb}\Delta E^{abs/emiss}(k,k')}{\hbar^2}}(z-z')\right) \tag{A9}$$

and $\Theta(\Delta E^{abs/emiss})$, which is the Heaviside function stating that $E_{1,\vec{k}} \geq V_{rb} - \hbar\omega_{LO}$ in the case of phonon absorption and that $E_{1,\vec{k}} \geq V_{rb} + \hbar\omega_{LO}$ in the case of phonon emission. These two conditions on the energy of the QW state clearly mean that the electron emission from the QW to the continuum is a thermoactivated process because only high-energy electron can make a phonon assisted transition.

The thermal average of the scattering time associated with absorption or emission of phonons is

$$\left\langle \frac{1}{\tau^{abs/emiss}} \right\rangle = \frac{2}{n_{QW}} \sum_{\vec{k}} \frac{1}{\tau^{abs/emiss}_{1,\vec{k}}} f_{QW}(E_{1,\vec{k}}). \tag{A10}$$

Hence, the characteristic rate for the thermionic emission can be expressed as

$$\frac{1}{\tau_{thermionic\ emi.}} = \left\langle \frac{1}{\tau^{abs}} \right\rangle + \left\langle \frac{1}{\tau^{emiss}} \right\rangle = \frac{\Omega C_F^2 m^*_{rb}}{8\pi^2\hbar^3}\sqrt{k_B T_{QW}} \times \left(n_{LO} e^{-\beta_{QW}(V_{rb}-E_1-\hbar\omega_{LO})} F_1^{abs}(T_{QW}) \times (n_{LO}+1) e^{-\beta_{QW}(V_{rb}-E_1+\hbar\omega_{LO})} F_1^{emiss}(T_{QW})\right), \tag{A11}$$

with

$$F_1^{abs/emiss} = \int_0^{\infty} dw e^{-w} \int_0^{\sqrt{w}} dv \int_0^{2\pi} d\theta \frac{N^{abs/emiss}(w,v,\theta)}{D^{abs/emiss}(w,v,\theta)}, \tag{A12}$$

$$N^{abs/emiss}(w,\nu,\theta) = \iint_{-\infty}^{\infty} dzdz'\chi_1^*(z)\chi_1(z')e^{-\left(D^{abs/emiss}(w,\nu,\theta)\sqrt{\frac{2m_{rb}^*}{\hbar^2}}|z-z'|\right)}\cos\left(\sqrt{\frac{2m_{rb}^*}{\hbar^2\beta_{QW}}}\nu(z-z')\right), \tag{A13}$$

$$D^{abs/emiss}(w,\nu,\theta) = \sqrt{\left(\Delta E_{emiss}^{abs} + \frac{w}{\beta_{QW}}\right)\frac{m^*}{m_{rb}^*} + \frac{(w-\nu^2)}{\beta_{QW}} - 2\sqrt{\left(\Delta E_{emiss}^{abs} + \frac{w}{\beta_{QW}}\right)\frac{m^*}{m_{rb}^*}\frac{(w-\nu^2)}{\beta_{QW}}}\cos(\theta)}, \tag{A14}$$

where w and ν are dimensionless variables and $\Delta E_{emiss}^{abs} = V_{rb} - E_1 \mp \hbar\omega_{LO}$.

2. Intra QW energy loss rate

In case of intrasubband transitions due to the absorption or emission of LO phonons, the scattering times for a QW electron in state $|1,\vec{k}\rangle$ read

$$\frac{1}{\tau_{1,\vec{k}}^{abs,intra}} = \frac{2\pi}{\hbar}n_{LO}\sum_{\vec{k'},\vec{Q},Q_z}\frac{C_F^2}{Q^2+Q_z^2}\left|\langle 1,\vec{k}\left|e^{i\vec{Q}\cdot\vec{\rho}}e^{iQ_z z}\right|1,\vec{k'}\rangle\right|^2\delta\left(E_{1,\vec{k'}} - E_{1,\vec{k}} - \hbar\omega_{LO}\right), \tag{A15}$$

$$\frac{1}{\tau_{1,\vec{k}}^{emiss,intra}} = \frac{2\pi}{\hbar}(n_{LO}+1)\sum_{\vec{k'},\vec{Q},Q_z}\frac{C_F^2}{Q^2+Q_z^2}\left|\langle 1,\vec{k}\left|e^{-i\vec{Q}\vec{\rho}}e^{-iQ_z z}\right|1,\vec{k'}\rangle\right|^2\delta\left(E_{1,\vec{k'}} - E_{1,\vec{k}} + \hbar\omega_{LO}\right). \tag{A16}$$

The summations over the phonon states lead to

$$\sum_{\vec{Q},Q_z}\frac{C_F^2\left|\langle 1,\vec{k}\left|e^{i\vec{Q}\cdot\vec{\rho}}e^{iQ_z z}\right|1,\vec{k'}\rangle\right|^2}{Q^2+Q_z^2} = \frac{C_F^2}{Q}\frac{L}{2}\iint_{-\infty}^{\infty}dzdz'\chi_1^2(z)\chi_1^2(z')e^{-Q|z-z'|} = \frac{LC_F^2}{2}\frac{I(Q)}{Q}, \tag{A17}$$

with $Q = \sqrt{k^2+k'^2-2kk'\cos(\theta)}$ and $\widehat{\vec{k},\vec{k'}} = \theta$, which, inserted in (A15) or (A16) and after integration on k', gives for phonon absorption,

$$\frac{1}{\tau_{1,\vec{k}}^{abs,intra}} = n_{LO}\frac{\Omega C_F^2}{4\pi}\frac{m^*}{\hbar^3}\int_0^{2\pi}d\theta\frac{I(Q)}{Q}, \tag{A18}$$

with $k'^2 = k^2 + 2m^*\omega_{LO}/\hbar$, and for phonon emission,

$$\frac{1}{\tau_{1,\vec{k}}^{emiss,intra}} = (n_{LO}+1)\frac{\Omega C_F^2}{4\pi}\frac{m^*}{\hbar^3}\int_0^{2\pi}d\theta\frac{I(Q)}{Q}\Theta(\hbar^2k^2/2m^* - \hbar\omega_{LO}), \tag{A19}$$

with $k'^2 = k^2 - 2m^*\omega_{LO}/\hbar$, where the Heaviside function express the minimum electron energy required for phonon emission.

The density of energy loss rate due to phonon absorption and emission is then calculated as

$$(P_{QW})_{intra\ QW} = \frac{2}{S}\sum_{\vec{k}}\left(\frac{\hbar\omega_{LO}}{\tau_{1,\vec{k}}^{abs,intra}} + \frac{-\hbar\omega_{LO}}{\tau_{1,\vec{k}}^{emiss,intra}}\right)f_{QW}(E_{1,\vec{k}})$$
$$= n_{QW}\frac{\Omega C_F^2\hbar\omega_{LO}}{4\pi\hbar^2}\sqrt{\frac{m^*}{2}}\left\{n_{LO} - (n_{LO}+1)e^{-\beta_{QW}\hbar\omega_{LO}}\right\}F_3(T_{QW}), \tag{A20}$$

with

$$F_3 = \int_0^{\infty}dwe^{-w}\int_0^{2\pi}d\theta\frac{N(w,\theta)}{D(w,\theta)}, \tag{A21}$$

$$N(w,\theta) = \iint_{-\infty}^{\infty}dzdz'\chi_1^2(z)\chi_1^2(z')e^{-\left(D(w,\theta)\sqrt{\frac{2m^*}{\hbar^2}}|z-z'|\right)}, \tag{A22}$$

$$D(w,\theta) = \sqrt{2wk_BT_{QW} + \hbar\omega_{LO} - 2\sqrt{wk_BT_{QW}(\hbar\omega_{LO}+wk_BT_{QW})}\cos(\theta)}. \tag{A23}$$

DATA AVAILABILITY

The data that support the finding of this work are within the article.

REFERENCES

[1]G. I. Meijer, Science **328**, 318 (2010).
[2]E. Pop and K. E. Goodson, J. Electron. Packaging **128**, 102 (2006).
[3]R. Rhyner and M. Luisier, Nano Lett. **16**, 1022 (2016).
[4]G. D. Mahan and L. M. Woods, Phys. Rev. Lett. **80**, 4016 (1998).
[5]G. D. Mahan, J. O. Sofo, and M. Bartkowiak, J. Appl. Phys. **83**, 4683 (1998).
[6]T. Zeng and G. Chen, Microscale Thermophys. Eng. **4**, 39–50 (2000).
[7]D. Vashaee and A. Shakouri, J. Appl. Phys. **95**, 1233–1245 (2004).
[8]A. Shakouri, C. LaBounty, J. Piprek, P. Abraham, and J. E. Bowers, Appl. Phys. Lett. **74**, 88 (1999).
[9]J. Zhang, N. G. Anderson, and K. M. Lau, IEEE Electron Device Lett. **25**, 345 (2004).
[10]K. A. Chao, M. Larsson, and A. G. Mal'shukov, Appl. Phys. Lett. **87**, 022103 (2005).
[11]X. Zhu, M. Bescond, T. Onoue, G. Bastard, F. Carosella, R. Ferreira, N. Nagai, and K. Hirakawa, Phys. Rev. Appl. **16**, 064017 (2021).
[12]E. Mykkänen, J. S. Lehtinen, L. Grönberg, A. Shchepetov, A. V. Timofeev, D. Gunnarsson, A. Kemppinen, A. J. Manninen, and M. Prunnila, Sci. Adv. **6**, eaax9191 (2020).
[13]A. Ziabari, M. Zebarjadi, D. Vashaee, and A. Shakouri, Rep. Prog. Phys. **79**, 095901 (2016).
[14]M. Bescond, D. Logoteta, F. Michelini, N. Cavassilas, T. Yan, A. Yangui, M. Lannoo, and K. Hirakawa, J. Phys. Condens. Matter **30**, 064005 (2018).
[15]A. Yangui, M. Bescond, T. Yan, N. Nagai, and K. Hirakawa, Nat. Commun. **10**, 4504 (2019).
[16]T. Jayasekera, K. Mullen, and M. A. Morrison, Phys. Rev. B **75**, 035316 (2007).
[17]M. Bescond, G. Dangoisse, X. Zhu, C. Salhani, and K. Hirakawa, Phys. Rev. Appl. **17**, 014001 (2022).
[18]A. E. P. Maia, A. P. C. P. Filho, A. J. C. Sampaio, and V. N. Freire, Phys. Status Solidi B **180**, 213–222 (1993).
[19]F. Caruso and D. Novko, Adv. Phys. X **7**, 1 (2022).
[20]J. Shah, A. Pinczuk, A. C. Gossard, and W. Wiegmann, Phys. Rev. Lett. **54**, 2045–2048 (1985).
[21]J. Shah, Solid State Electron. **21**, 43–50 (1978).
[22]C. R. H. White, M. S. Skolnick, L. Eaves, M. L. Leadbeater, M. Henini, O. H. Hughes, G. Hill, and M. A. Pate, Phys. Rev. B. **45**, 6721–6730 (1992).
[23]R. Lake and S. Datta, Phys. Rev. B. **45**, 6670–6685 (1992).
[24]S. Datta, *Electronic Transport in Mesoscopic Systems* (Cambridge University Press, 2013).
[25]G. Bastard, *Wave Mechanics Applied to Semiconductor Heterostructures* (Les ○Editions de Physique, Les Ulis, 1988).